


 Cite this: *RSC Adv.*, 2021, 11, 4365

 Received 5th November 2020  
 Accepted 18th December 2020

DOI: 10.1039/d0ra09408k

[rsc.li/rsc-advances](http://rsc.li/rsc-advances)

# Endowing magnesium with the corrosion-resistance property through cross-linking polymerized inorganic sol–gel coating†

 Wei Wang,  Xiao-Na Yang, Yang Wang, Yong Fan  and Jia-Ning Xu\*

The design of a highly adhesive, defect-free and low-temperature sol–gel coating for the protection of magnesium alloys is desirable yet challenging. In this study, a novel SiO<sub>2</sub>-based sol–gel coating is developed by a ring-opening addition reaction. Notably, the integration of individual sol clusters endows the sol–gel coating with a smooth and compact surface morphology, and eliminates the potential corrosion site of the low-temperature-prepared sol–gel coating. Besides, the as-obtained sol–gel coating exhibits excellent metallic adhesion nature. Most importantly, it increases the overall impedance modulus by 27 times than that of the conventional strategy and decreases the corrosion rate from 3.8 ± 0.5 mg cm<sup>-2</sup> per day (commercial chromate conversion coating) to 0.5 ± 0.2 mg cm<sup>-2</sup> per day.

## 1. Introduction

While magnesium (Mg) alloys have attracted considerable attention owing to their excellent mechanical and biological properties, the poor corrosion-resistance property has brought numerous obstacles to the application of Mg alloys.<sup>1–3</sup> The oxide coating prepared by the sol–gel technology outperforms other methods in terms of high adhesion with a metallic substrate, and superior corrosion-resistance.<sup>4,5</sup> However, the conventional preparation process requiring high-temperature annealing process (400–800 °C) brings additional thermal energy consumption and undesirable changes in the microstructure of heat-sensitive Mg alloys (melting point, ~650 °C).<sup>6</sup> Moreover, cracks and other physical defects are inevitable in the oxide-based sol–gel coating due to the evaporation of catalysts (hydrochloric acid, nitric acid or acetic acid, *etc.*) in the thermal treatment, which provides numerous vulnerable sites for initiating corrosion.<sup>7</sup> Although researchers have developed numerous preparation strategies to avoid the thermal process, these strategies had to be carried out at the expense of metallic adhesion and/or environmental pollution.<sup>8–10</sup> Therefore, a method to prepare corrosion-resistant sol–gel coating under mild and environmentally benign conditions is urgently needed.

In the preparation process of the sol–gel coating, the high-temperature treatment aims to increase the interaction between sol clusters and stabilize physical and chemical properties.<sup>6,7</sup> Recently, click chemistry has become one of the most

powerful paradigms in the synthesis and modification of materials.<sup>11</sup> Among these, the ring-opening addition reaction (AORA) of epoxy groups is broadly applied in the synthesis of polymer matrices and in the introduction of functional group.<sup>12,13</sup> Thus, we hypothesized that the physical integration and subsequent corrosion protection of sol–gel coatings can be improved by the AORA of epoxy groups that polymerize each of the relatively independent clusters. The polymeric hybridization nature of clusters is highly likely to have a trivial impact on the coating bonding strength of the metal substrate.

Herein, AORA as an isolated parameter was studied on a SiO<sub>2</sub> based sol–gel coating to establish its role in the anti-corrosion performance by taking a neat Mg as a model metallic material due to its simple composition. In brief, epoxy groups were introduced into the precursor sol of ZrO<sub>2</sub> and SiO<sub>2</sub> via 3-glycidyloxypropyltrimethoxysilane, and then cured by a small amount of 2-methylimidazole at a low temperature (≤80 °C). Owing to the polymerization process of introduced epoxy groups, the surface morphology of the obtained coating is very smooth, flat and crack-free than that of the conventionally prepared sol–gel coating. More importantly, unchanged covalent-bond-based binding characteristics maintain a high adhesion level of the modified sol–gel coating (the highest level in the ISO-2049:2013 standard). As expected, the modified sol–gel coating shows excellent performance in corrosion resistance compared with that of conventional sol–gel coatings and commercial chromate conversion coatings.

## 2. Experimental section

### 2.1. Chemicals

All chemicals were commercially available and used as received in the present study. Tetraethoxysilane (TEOS, 99%), 3-

College of Chemistry, Jilin University, Changchun 130012, China. E-mail: xujn@mail.jlu.edu.cn

† Electronic supplementary information (ESI) available. See DOI: 10.1039/d0ra09408k



glycidyoxypropyltrimethoxysilane (GPTMS, 97%), zirconyl chloride octahydrate ( $\text{ZrOCl}_2 \cdot 8\text{H}_2\text{O}$ , 99%), isopropyl alcohol (99.5%), absolute ethanol (99.7%) and 2-methylimidazole (98%) were all purchased from Aladdin Bio-Chem Technology Co. Ltd., Shanghai, China. Hydrochloric acid (HCl, 36.0–38.0 wt%), sodium chloride (NaCl, 98%), sodium dichromate dihydrate ( $\text{Na}_2\text{Cr}_2\text{O}_7$ , 99.5%), magnesium fluoride ( $\text{MgF}_2$ , 98%), ammonium bifluoride ( $\text{NH}_4\text{HF}$ , 98%), chromium trioxide ( $\text{CrO}_3$ , 99%), silver nitrate ( $\text{AgNO}_3$ , 99.8%), barium nitrate ( $\text{Ba}(\text{NO}_3)_2$ , 99.5%) and acetone (99.5%) were supplied by Beijing Chemical Reagents Co. Ltd., China.

## 2.2. Mg substrate specimens

High purity Mg specimens (>99.9%,  $\text{Fe} \leq 40$  ppm) were cut off from an as-cast ingot into  $15 \times 15 \times 3$  mm<sup>3</sup> square pieces. The specimen was mechanically ground with silicon carbide papers progressively up to 2000-grit surface finish and running water as the lubricant, and ultrasonically cleaned in acetone and absolute ethanol for 30 min. Subsequently, the Mg specimen was immersed in 1 M NaOH aqueous solution at 80 °C for 4 h to create a thin layer of porous  $\text{Mg}(\text{OH})_2$  to improve the adhesion for subsequent sol-gel coating, followed by rinsing with deionized water and ethanol, and then dried under a high pressure nitrogen flow.

## 2.3. The preparation of commercial chromate conversion coating

According to an open publication,<sup>14</sup> an aqueous solution containing 120 g L<sup>-1</sup>  $\text{Na}_2\text{Cr}_2\text{O}_7$  and 2.5 g L<sup>-1</sup>  $\text{MgF}_2$  was prepared to produce commercial chromate coatings on the Mg substrate for comparison. Before exposing to the chromate solution, the Mg substrate was immersed into an aqueous solution containing 50 g L<sup>-1</sup>  $\text{NH}_4\text{HF}$  for 300 s to activate its surface. Thereafter, the Mg substrate was placed in the aforementioned boiled chromate solution for 30 min, followed by rinsing with hot water (60–70 °C) and dried under airflow at room temperature, and thus named as the CM coating.

## 2.4. The preparation of $\text{SiO}_2$ @ $\text{ZrO}_2$ sol-gel coatings

The preparation process of the sol-gel coating was optimized according to the method in the ESL.<sup>†</sup> Briefly, 4.73 mL TEOS (19.76 mmol) was added into a mixed solvent composed of 2.5 mL ethanol and 2.5 mL isopropyl alcohol. Thereafter, 335.1 mg  $\text{ZrOCl}_2$  (1.04 mmol,  $n_{\text{Si}} : n_{\text{Zr}} = 5 : 95$ ) was added into the solution. When all solid substances were dissolved, 375  $\mu\text{L}$  HCl aqueous solution (20.8 mmol  $\text{H}_2\text{O}$ , pH = 2) and 3.96 mL GPTMS (15.7 mmol) were transferred drop-wise into the clear solution. The pH value of the HCl solution used in the preparation procedure was monitored using an electrolyte-type pH meter (PB-10, Sartorius, Germany). Finally, 20 mg 2-methylimidazole (0.244 mmol) was added. Magnetic stirring was applied to all procedures. The as-prepared solution was hydrolyzed and polymerized at room temperature for 1 h to obtain the sol. A dip coating technique was employed to grow  $\text{SiO}_2$ @ $\text{ZrO}_2$  (designated as SiZr-GH hereafter) sol-gel coatings on the surface of Mg specimens. In brief, the Mg piece was fully

immersed in the sol for 10 s and lift up vertically through an electric-motor-driven arm at a speed of 1 cm min<sup>-1</sup>. Thereafter, SiZr-GH sol-covered Mg species were cured in an oven at 80 °C for 4 h. In addition, 2-methylimidazole-free sol-gel coatings (SiZr-G), and GPTMS- and 2-methylimidazole-free sol-gel coatings (SiZr) were prepared as controls for comparison.

## 2.5. The measurement of physical and chemical features

Sol-gel coatings were characterized *via* Fourier transform infrared spectroscopy (FTIR, Nicolet™ iS™ 10, ThermoFisher Scientific, US), X-ray photoelectron spectroscopy (XPS, ESCALAB™, ThermoFisher Scientific, USA) and scanning electron microscopy (SEM, SU8020, HIACHI, Japan).

The reaction progress of SiZr-GH sol-gel coatings were evaluated by FTIR and spectra were recorded over a range of 4000–400 cm<sup>-1</sup>. Samples were prepared in two different ways: (a) no curing: sol solution droplet on KBr disc; and (b) cured: part of sol-gel coating was mixed with KBr powder and compressed into disc. The surface morphology of samples was revealed through SEM high-resolution images.

In the XPS study, photoelectrons generated by Al K $\alpha$  (1486.6 eV) primary radiation (20 kV, 15 mA) were analyzed with a hemispherical analyzer, and core level XPS spectra for Si 2p, Zr 3d, Mg 2p, O 1s and C 1s were recorded and fitted. Binding energy was calibrated with the standard C 1s (hydrocarbon C–C, C–H) value of 285 eV. Data were quantitatively assessed using a one-way factorial analysis of the variance method.

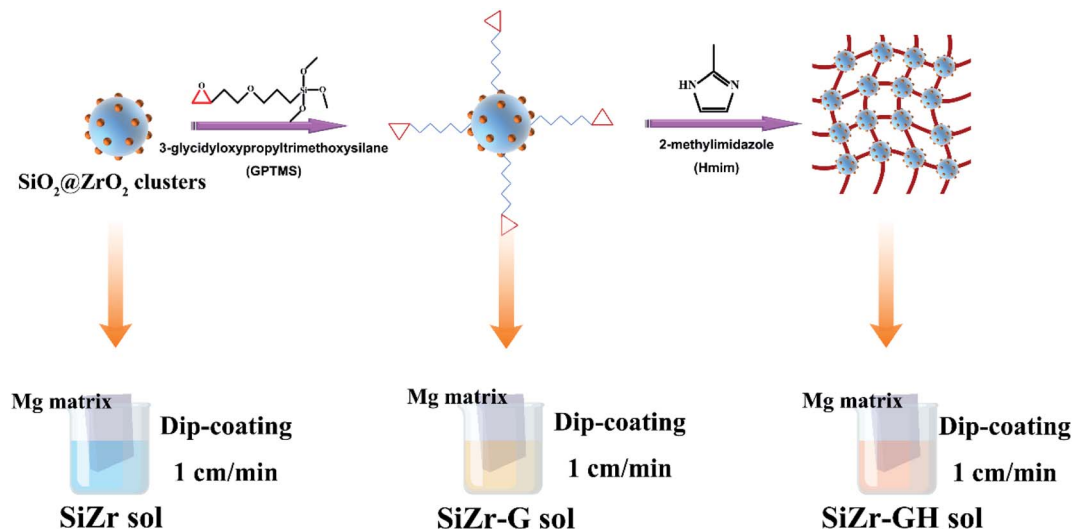
## 2.6. Adhesion strength testing

The adhesion of substrates and coatings was determined referring to a standard ISO-2049:2013 cross-cut test.<sup>15</sup> In brief, a 100-cell grid was drawn out on a sol-gel coating with a spacing of 1 mm between grid blades. Then, a transparent adhesive tape (Cat. 600, 3 M) was firmly placed upon the affected area, followed by quick peeling off to observe the remaining surface of the coating with an optical microscope. The adhesion level was determined by the ratio of the area of remaining coating to that of the original coating, and the larger ratio indicates the high adhesion level.

## 2.7. Analysis of electrochemical performance

For electrochemical tests, a “flat-cell” (F030, Tianjin Ida, China) equipped with an exposed working electrode (Mg specimens) of area 1 cm<sup>2</sup>, and Ag/AgCl and a Pt mesh as reference and counter electrodes, respectively, containing 300 mL of NaCl (0.6 M) electrolyte was used. Electrochemical experiments were performed on a CHI760E (CH Instruments, China) potentiostat/galvanostat using the CHI 16.06 software at a sweeping rate of 10 mV s<sup>-1</sup>. Potentiodynamic polarization curves were recorded after 10 min stabilization at an open circuit potential (OCP) and used to estimate the corrosion potential ( $E_{\text{corr}}$ ) and corrosion current density ( $i_{\text{corr}}$ ) *via* Tafel fitting using the CHI 16.06 software. In general, a portion of the curve that commences >50 mV from the corrosion potential was selected, and  $E_{\text{corr}}$  and  $i_{\text{corr}}$  were subsequently estimated from the value where the fit intercepted the potential value of the true corrosion potential. A minimum of five replicate scans were performed for each





Scheme 1 The schematic of reaction processes and modified sol-gel coating.

material group to ensure reproducibility. Electrochemical impedance spectroscopy (EIS) was conducted over a frequency range from 100 kHz to 10 mHz, with a sinusoidal amplitude of 10 mV and same after 10 min of OCP conditioning. EIS data were analyzed using ZSimpWin (version 3.10) software. All electrochemical tests were carried out in a Faraday cage to avoid interferences.

## 2.8. Mass loss in aqueous NaCl electrolyte

To examine the long-term corrosion performance of coatings, mass loss was carried out in 0.6 M NaCl at room temperature for 28 days. The exposed surface area of each specimen in contact with 10 mL NaCl solution was constantly set as 6.3 cm<sup>2</sup>. After immersion, specimens were removed from the NaCl electrolyte and cleaned in a solution containing 200 g L<sup>-1</sup> CrO<sub>3</sub>, 20 g L<sup>-1</sup> AgNO<sub>3</sub> and 10 g L<sup>-1</sup> Ba(NO<sub>3</sub>)<sub>2</sub> for 1 min at room temperature to remove corrosion products from the surface, according to industrial standards ISO-8407:2009.<sup>16</sup> The variations of mass after immersion and cleaning procedures were divided by the surface area of specimens and immersion time to yield mass loss rate (mg cm<sup>-2</sup> per day). Three minimal replicates were carried out for each data point to ensure reproducibility ( $n = 3$ ).

## 2.9. Statistical analysis

All quantitative results were expressed as mean  $\pm$  standard deviation (SD). Statistical significance was determined by Student's *t*-test and one-way ANOVA. Differences between the groups of \**p* values (<0.05) were considered statistically significant.

# 3. Results and discussion

## 3.1. Formation mechanism of the modified sol (SiZr-GH) coating

Scheme 1 illustrates the detailed procedure for the preparation of SiZr-GH sol-gel coating. Firstly, a mixture of tetraethoxysilane (TEOS) and zirconia chloride (ZrOCl<sub>2</sub>) was hydrolyzed in

the mixed solvent of ethanol and isopropyl alcohol (volume ratio, 1 : 1) to form the precursor sol. Thereafter, 3-glycidyloxypropyltrimethoxysilane (GPTMS) was drop-wise added into the above solution for introducing the epoxy groups on the sol clusters at room temperature. Afterward, 2-methylimidazole (curing agent) was added under magnetic stirring and then the solution was coated upon the Mg substrates by the dip-coating technology. Finally, the sol-gel coating was cured at 80 °C in an oven for 4 h.

FTIR spectra were recorded to determine the occurrence of the ring-opening addition reaction during the preparation process of SiZr-GH coating. As depicted in Fig. 1, the stretching vibration absorption peaks of the epoxy group at about 910 cm<sup>-1</sup> disappeared after the curing step. Such variations indicate that epoxy groups experienced a ring-opening addition reaction when 2-methylimidazole was added, which led to the chemical bonding of individual clusters and may increase the cross-linking density of the SiZr-GH sol.

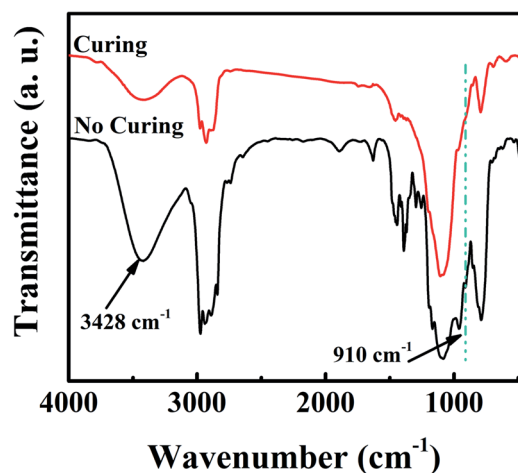


Fig. 1 The FTIR spectra of SiZr-GH sol before and after the curing process.



The increase in cross-linking density will result in a compact, continuous and defect-free surface morphology,<sup>17–19</sup> which is highly desirable to play an inhibitory role in controlling the corrosion behaviour of underlying metal components.<sup>20</sup> Accordingly, we observed variations in the surface morphology of the sol-gel coating prior to and after GPTMS and 2-methylimidazole modification by scanning electron microscopy (SEM) and energy dispersive spectroscopy (EDS). The surface of the modified free sol-gel coating (SiZr) exhibited pronounced cracks and a great number of scattering particles with regular edges (Fig. 2a). Alternatively, as shown in Fig. 2b, the number of these particles was significantly reduced on the surface of the GPTMS-improved sol-gel coating (SiZr-G). The surface morphology was further improved by the modification of GTPMS and 2-methylimidazole (SiZr-GH); the ultimate target, *i.e.*, sol-gel coating, presents a dense, continuous and smooth surface (Fig. 2c). This suggests that the ring-opening addition reaction polymerization strategy is beneficial in restraining the formation of physical defects in the sol-gel coating prepared at room temperature. In addition, scattering particles with regular edges that upon SiZr and SiZr-G sol-gel coating, have been determined to mainly magnesium oxide through EDS mapping. Owing to the limited cross-linking density of the sol-gel coating prepared at a low temperature, it is relatively loose in most cases,<sup>20</sup> which leads to the reaction between the Mg substrate and oxygen to obtain these particles mainly made of magnesium oxide. In summary, the smooth and defect-free surface of the SiZr-GH sol-gel coating set a fundamental basis for further application.

### 3.2. Coating adhesion strength

A high bonding strength of the sol-gel coating towards an underlying metal substance is crucial for its protective role in

corrosive conditions over a sufficient time frame.<sup>21–23</sup> In general, existing low-temperature modification approaches for the preparation of the sol-gel coating involve macromolecular polymer compounds, which tend to have adverse effects on the adhesion of the sol-gel coating.<sup>24,25</sup> To validate the metallic adhesion of the modified sol-gel coating, cross-cut tests were conducted. Results displayed in Fig. 3a–c evidently indicate that the adhesion strength of SiZr, SiZr-G and SiZr-GH sol-gel coatings upon Mg specimens was ascertained as grade 0, which is the highest level of coating based on ISO-2049:2013 standards.<sup>15</sup> From the cross-sectional SEM images (Fig. 3d–f), there is no clear dividing line between the coating and Mg substrates and possessed a continuous, uniform and compact morphology. The ring-opening addition reaction-based preparation process avoided significant interface separation and adhesive property damages compared to the polymer hybrid sol-gel coating.

In addition, X-ray photoelectron spectroscopy (XPS) was used to further study the influence of the modification process on covalent-bond-based binding characteristics of the sol-gel coating. The XPS spectrum demonstrates that numerous covalent oxygen bonds existed in the SiZr-GH sol-gel coating (Fig. 4), and Mg–O bonds especially provide a chemical path for the sol-gel coating to bind with the metal substrate (pure Mg), which is consistent with the binding characteristic of the conventional sol-gel coating.<sup>26</sup> A balance between mild preparation conditions and the metallic adhesion was created by our preparation strategy, which eliminates the potential corrosion site without changing the adhesion property of the sol-gel coating.

### 3.3. Electrochemical analysis for corrosion-resistance performance

In the following part, the corrosion protection performance of the as-prepared sol-gel coating was evaluated *via*

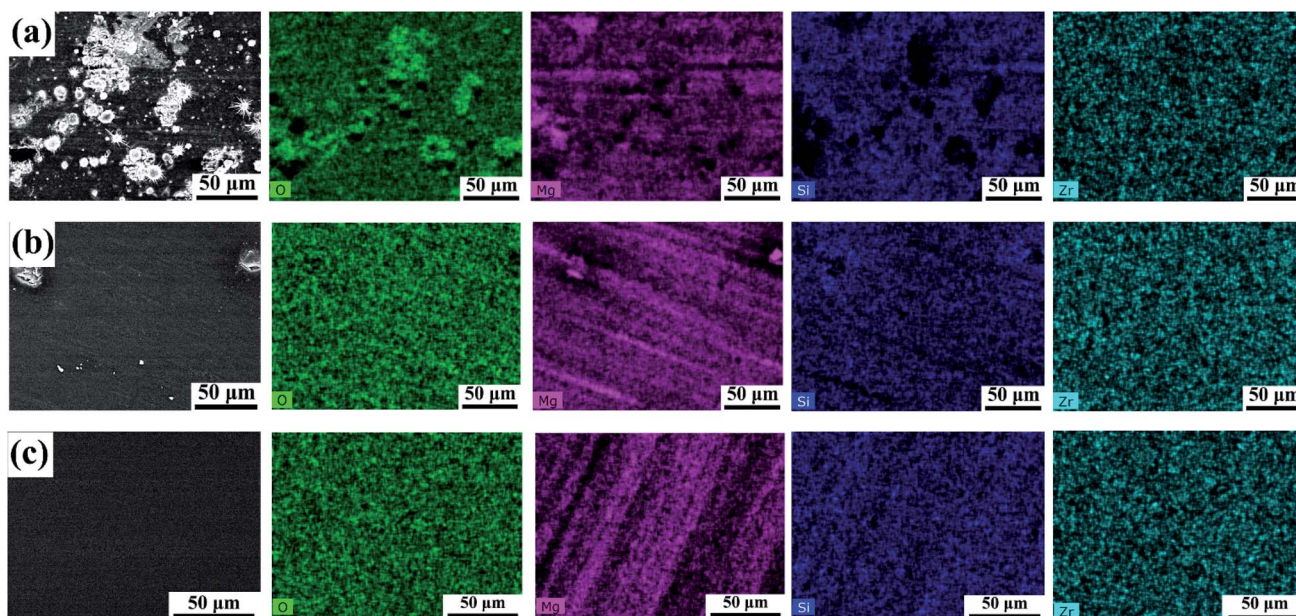


Fig. 2 SEM and EDS mapping images of the as-prepared sol-gel coating. (a) Modified free sol-gel coating (SiZr), (b) GPTMS-modified sol-gel coating (SiZr-G) and (c) GTPMS and 2-methylimidazole-modified sol-gel coating (SiZr-GH).



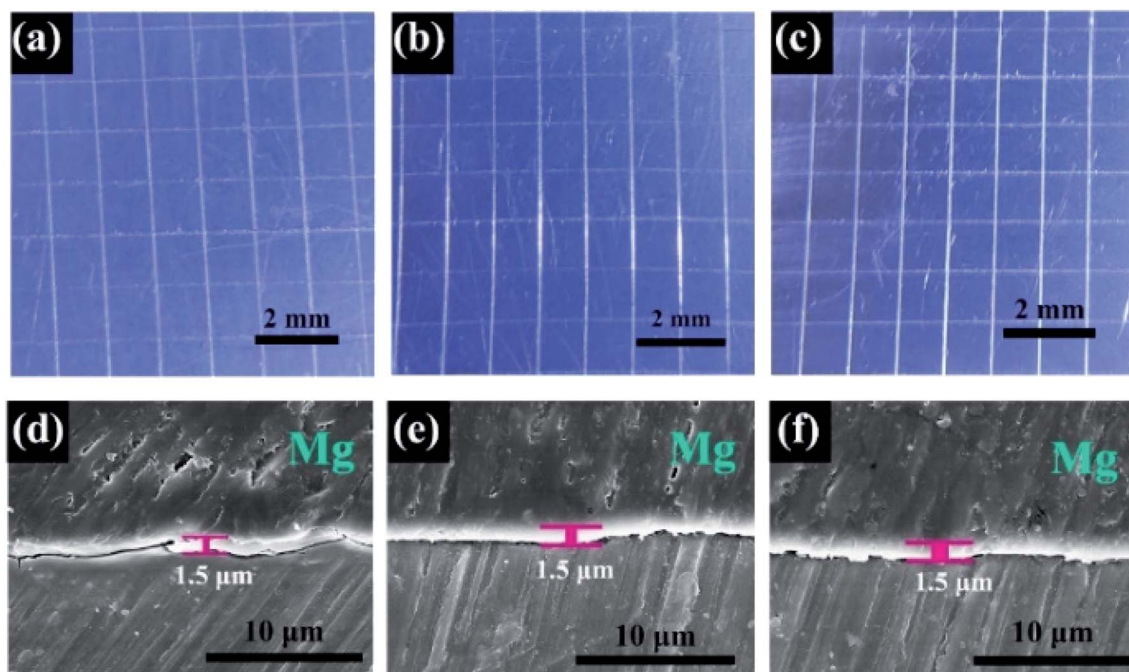


Fig. 3 (a–c) Optical photographs of the surface of (a) SiZr, (b) SiZr-G and (c) SiZr-GH sol-gel coatings on pure Mg substrate after designated adhesion tests through the cross-cut test according to the standards of ISO-2049:2013.<sup>15</sup> SEM images of the cross-sectional micrography, (d) SiZr, (e) SiZr-G and (f) SiZr-GH sol-gel coating.

electrochemical tests and was compared with that of the conventional sol-gel coating and commercial coating. Potentiodynamic polarization (PDP) curves are a common technique to quantify the instant corrosion kinetics of bare and coated Mg specimens in a corrosive electrolyte, such as the NaCl solution.<sup>27–31</sup> To examine the protective function of SiZr-GH sol-gel coatings on pure Mg, PDP curves were recorded in a 0.6 M neutral NaCl solution over a potential range from  $-150$  mV to  $600$  mV vs. the open circuit potential (OCP). It is evident that the polarization curves of all coatings shifted to the lower corrosion current density region and both cathodic and anodic current densities reduced but to different extents (Fig. 5a). This illustrates that the corrosion of Mg is kinetically inhibited since the cathodic branch is assumed to represent the hydrogen

evolution through water reduction and the anodic branch is related to the Mg dissolution.<sup>32</sup> The  $i_{\text{corr}}$  of all coatings showed a reduction in comparison with that of the neat Mg specimen, as well as a further decrease on the SiZr-GH coating by an order of magnitude. This benefits individual sol clusters integrated by the ring-opening addition reaction, which improves the surface morphology of the SiZr-GH coating and eliminates the potential corrosion sites (Fig. 2). Moreover, the  $i_{\text{corr}}$  of pure Mg increases gradually with the surface morphology of the sol-gel coating upon its top deterioration (e.g. SiZr-G and SiZr), which proves the above conjecture.

EIS measurements were collected immediately following 10 min stabilization at OCP during exposure to the 0.6 M neutral NaCl solution. The high-frequency ( $1-10^5$  Hz) loop

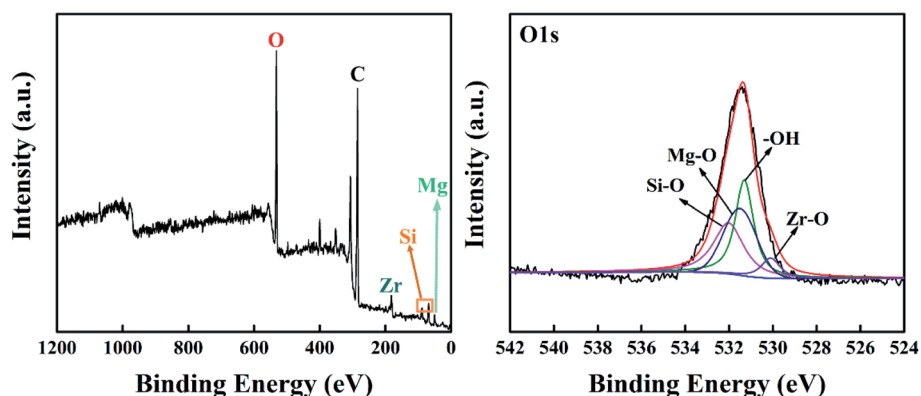
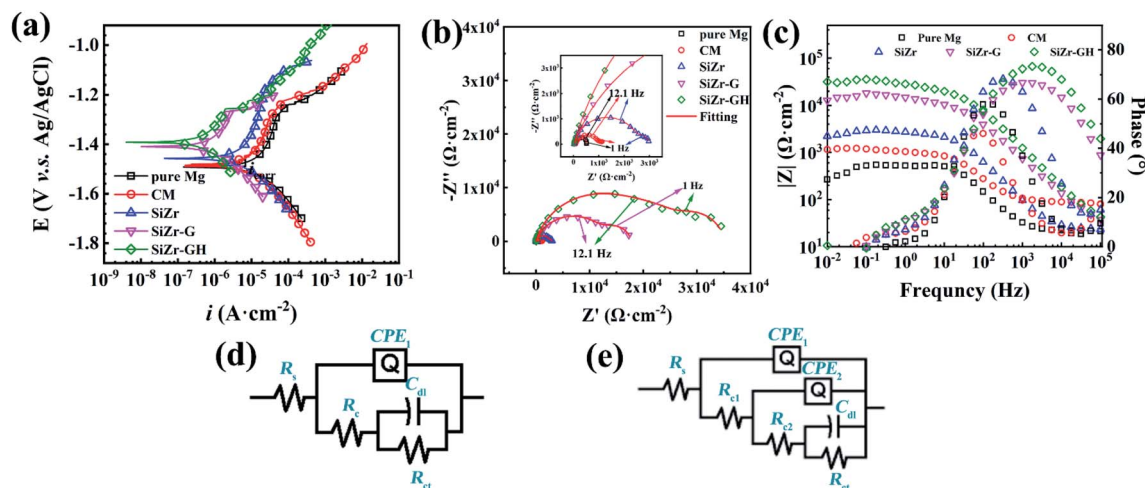


Fig. 4 XPS survey spectra and O1s peak-fitted curves of the surface of SiZr-GH sol-coated pure Mg.





**Fig. 5** (a) Potentiodynamic polarization curves of bare Mg and various coatings obtained at a sweep rate of  $10 \text{ mV s}^{-1}$ ; (b) the estimated average value of  $E_{\text{corr}}$  and  $i_{\text{corr}}$  through Tafel fitting extrapolation via CHI 16.06 software ( $n = 5$ ); EIS plots in (a) Nyquist and (b) Bode formats with corresponding fitting data collected over a period of 30 min (after 10 min OCP stabilization) ( $n = 3$ ) over a range of frequency from 100 kHz to 10 mHz; equivalent circuit used to fit the EIS data of (c) pure Mg specimen, and (d) chromate conversion coating and sol-gel coating. (e), but this does not appear to be mentioned in the caption. Would you like to modify the caption or resupply the artwork (preferably as a TIF file at 600 dots per inch)?

corresponds to the charge resistance of materials, whilst the response from the electrochemical double layer can be reflected by the semi-circle located in the low-frequency range (0.01–1 Hz).<sup>33,34</sup> From Nyquist plots in Fig. 5b, the high-frequency loop of the SiZr-GH sample is larger than other coatings sharply increasing in the order of pure Mg < CM < SiZr < SiZr-G < SiZr-GH. Furthermore, the value of  $|Z|_{0.01 \text{ Hz}}$  is an essential indicator for assessing the corrosion resistance of materials and represents the value of the overall impedance modulus.<sup>35,36</sup> From Bode plots in Fig. 5c, the  $|Z|_{0.01 \text{ Hz}}$  value of the SiZr-GH sample ( $31.9 \text{ k}\Omega \text{ cm}^{-2}$ ) increased by approximately 27 times compared to that of CM ( $1.2 \text{ k}\Omega \text{ cm}^{-2}$ ) and conventional SiZr sol-gel coating ( $2.2 \text{ k}\Omega \text{ cm}^{-2}$ ). Furthermore, we proposed several equivalent circuits (Fig. 5d and e) to fit EIS results:  $R_s(\text{CPE}_1(R_c(C_{\text{dl}}R_{\text{ct}})))$  was used for fitting the EIS data of pure Mg, and  $R_s(\text{CPE}_1(R_{\text{c1}}(\text{CPE}_2(R_{\text{c2}}(C_{\text{dl}}R_{\text{ct}}))))$  was used for fitting the EIS data of CM and sol-gel coatings. In these circuits,  $R_s$  represents the solution resistance;  $C_{\text{dl}}$  and  $R_{\text{ct}}$  represent the double-layer capacitance and charge transfer resistance, respectively; CPE

represents the capacitance of the film effect and  $R_c$  represents the total resistance of pores or coating. The polarization resistance ( $R_p$ ), which is the sum of  $R_{\text{ct}}$  and  $R_c$ , is proposed to evaluate the corrosion resistance. The fitting data (Table 1) further indicate that the ring-opening addition reaction-modified sol-gel coating endowed neat Mg with desired corrosion-resistance performance, which was due to the integration of sol clusters and the improvement of surface morphology.

### 3.4. Long-term corrosion-resistance performance

Though electrochemical techniques provided critical information regarding instant anodic dissolution kinetics and interfacial states of the sol-coated pure Mg specimens, direct evidence in terms of the long-term corrosion progress of coated Mg parts is also essentially desired. In this regard, the long-term corrosion behavior of coating-protected pure Mg was explored *via* mass loss tests in the 0.6 M neutral NaCl solution for 28 days. Three groups of coatings were designed to assess the possible

**Table 1** The fitting result of EIS depicted in Fig. 5c

	Pure Mg	CM	SiZr	SiZr-G	SiZr-GH
$R_s$ ( $\Omega \text{ cm}^{-2}$ )	21.91	0.01	1.489	22.79	25.42
$R_{\text{c1}}$ ( $\Omega \text{ cm}^{-2}$ )	158.8	91.47	22.78	$1.345 \times 10^4$	$2.186 \times 10^4$
$\text{CPE}_1$	$F \text{ cm}^{-2} \text{ s}^{1-n}$	$7.398 \times 10^{-7}$	$2.427 \times 10^{-8}$	$1.526 \times 10^{-6}$	$5.335 \times 10^{-7}$
$n$	0.9389	0.8097	0.9668	0.773	0.8359
$R_{\text{c2}}$ ( $\Omega \text{ cm}^{-2}$ )	—	932.6	2595	4305	8021
$\text{CPE}_2$	$F \text{ cm}^{-2} \text{ s}^{1-n}$	$1.692 \times 10^{-5}$	$5.467 \times 10^{-6}$	$4.969 \times 10^{-5}$	$8.701 \times 10^{-6}$
$n$	—	0.8492	0.87	0.9146	0.8089
$C_{\text{dl}}$ ( $F \text{ cm}^{-2}$ )	$4.996 \times 10^{-6}$	$2.941 \times 10^{-3}$	$5.973 \times 10^{-3}$	$7.191 \times 10^8$	$4.28 \times 10^{-5}$
$R_{\text{ct}}$ ( $\Omega \text{ cm}^{-2}$ )	35.72	143.3	380.4	$6.168 \times 10^6$	5294
Chi-squared	$1.86 \times 10^{-3}$	$2.53 \times 10^{-4}$	$9.15 \times 10^{-5}$	$8.41 \times 10^{-4}$	$9.87 \times 10^{-4}$



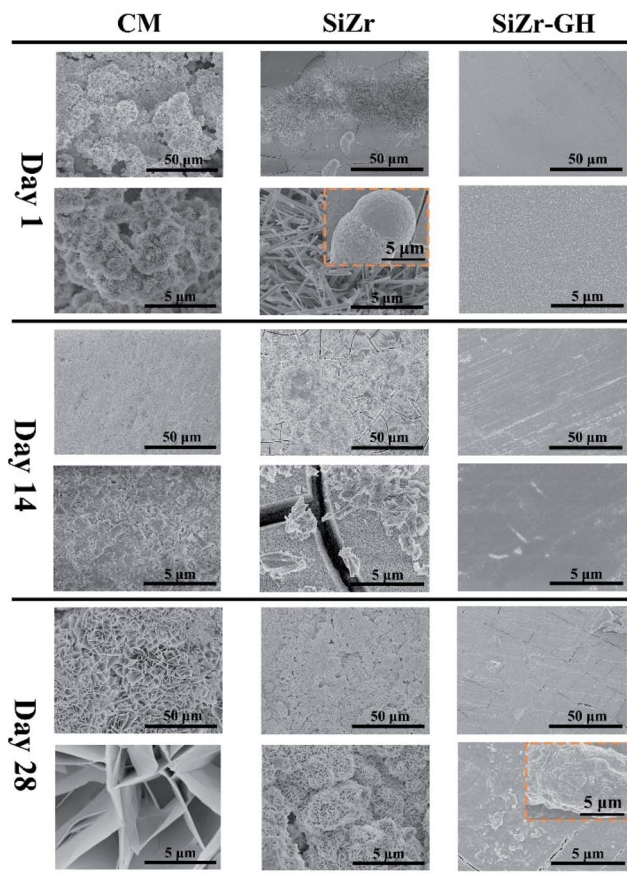


Fig. 6 Top-view secondary electron scanning microscopy graphs of various coating samples after immersion in 0.6 M neutral NaCl for 1, 14 and 28 days.

contributions from each individual factor to corrosion protection property, namely commercial chromate conversion coating (CM), SiZr and SiZr-GH. The SEM observation (Fig. 6) qualitatively indicates that the corrosion resistance is in the order of SiZr-GH > SiZr > CM. After exposure to the NaCl solution for 28

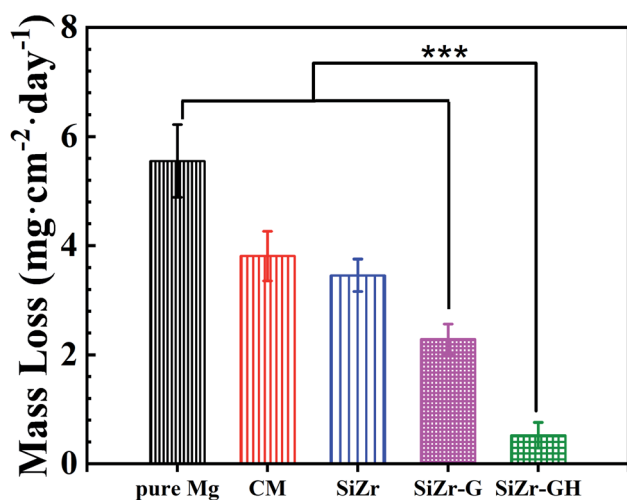


Fig. 7 The mass loss of various coatings after exposure to 0.6 M neutral NaCl solution for 28 days ( $n = 3$ ,  $***p < 0.001$ ).

days, a small number of corrosion products were generated on the surface of SiZr-GH, while SiZr and CM accumulated a large amount of platelet-shaped corrosion products in a loose manner. Thus, this suggests the following points: (a) sol-gel coating demonstrates better corrosion resistance than that of the commercial chromate conversion coating, and (b) our designed sol-gel coating preparation strategy exhibits great improvement in the corrosion protection property.

In terms of the quantitative study of corrosion resistance, the mass loss test was utilized. As shown in Fig. 7, the SiZr-GH coating exhibits the least mass loss ( $0.5 \pm 0.2 \text{ mg cm}^{-2}$  per day), whilst bare Mg displays the highest mass loss rate ( $5.6 \pm 0.7 \text{ mg cm}^{-2}$  per day). The protective function of SiZr-G ( $2.3 \pm 0.3 \text{ mg cm}^{-2}$  per day) is inferior to that of SiZr-GH, though remains better than CM ( $3.8 \pm 0.5 \text{ mg cm}^{-2}$  per day) and SiZr ( $3.5 \pm 0.3 \text{ mg cm}^{-2}$  per day). While the addition of GPTMS only can improve the corrosion resistance (SiZr-G) to a certain extent, the corrosion resistance performance has been greatly improved after the addition of 2-methylimidazole (the curing agent of epoxy groups) (SiZr-GH). This is due to the integration of clusters and improvement in the surface morphology, and is consistent with electrochemical test results.

## 4 Conclusions

In summary, we have designed and synthesized a SiO<sub>2</sub>-based sol-gel coating by applying low-temperature ring-opening addition reaction as the preparation process. The polymerization of individual clusters under mild hydrolysis and curing conditions results in a compact, continuous and defect-free surface morphology. Especially, the outstanding metallic adhesion nature of the sol-gel coating was not damaged in the modified process. Finally, the sol-gel coating shows excellent corrosion resistant performance, which enables to increase the overall impedance modulus by 27 times than that of the conventional sol-gel coating and decrease the corrosion rate from  $3.8 \pm 0.5 \text{ mg cm}^{-2}$  per day (commercial chromate conversion coating) to  $0.5 \pm 0.2 \text{ mg cm}^{-2}$  per day. This strategy opens great perspectives in designing novel and efficient corrosion resistant sol-gel coatings and might shed light on the exploration of powerful protocols to address the limited application problems of magnesium alloys.

## Conflicts of interest

There are no conflicts to declare.

## Acknowledgements

The authors are grateful for grants received from the National Natural Science Foundation of China (Grant No. 51875240).

## References

- 1 S. Tang, T. Xin, W. Xu, D. Miskovic, G. Sha, Z. Quadir, S. Ringer, K. Nomoto, N. Birbilis and M. Ferry, *Nat. Commun.*, 2019, **10**, 1–8.



- 2 T. T. Trang, J. H. Zhang, J. H. Kim, A. Zargarani, J. H. Hwang, B. C. Suh and N. J. Kim, *Nat. Commun.*, 2018, **9**, 1–6.
- 3 P. Xiong, Z. Jia, W. Zhou, J. Yan, P. Wang, W. Yuan, Y. Li, Y. Cheng, Z. Guan and Y. Zheng, *Acta Biomater.*, 2019, **92**, 336–350.
- 4 M. Faustini, L. Nicole, E. Ruiz-Hitzky and C. Sanchez, *Adv. Func. Mater.*, 2018, **28**, 1704158–1704188.
- 5 E. V. Skorb, D. Fix, D. V. Andreeva, H. Möhwald and D. G. Shchukin, *Adv. Func. Mater.*, 2009, **19**, 2373–2379.
- 6 Q. Lei, J. Guo, A. Nouredine, A. Wang, S. Wuttke, C. J. Brinker and W. Zhu, *Adv. Func. Mater.*, 2020, **30**, 1909539–1909567.
- 7 K. Wang and J. He, *ACS Appl. Mater. Interfaces*, 2018, **10**, 11189–11196.
- 8 M. L. Zheludkevich, R. Serra, M. F. Montemor, K. A. Yasakau, I. M. M. Salvado and M. G. S. Ferreira, *Electrochim. Acta*, 2005, **51**, 208–217.
- 9 Q. Li, X. Zhong, J. Hu and W. Kang, *Prog. Org. Coat.*, 2008, **63**, 222–227.
- 10 N. Li, Y. D. Li, Y. B. Wang, M. Li, Y. Cheng, Y. H. Wu and Y. F. Zheng, *Surf. Interface Anal.*, 2013, **45**, 1217–1222.
- 11 W. Xi, T. F. Scott, C. J. Kloxin and C. N. Bowman, *Adv. Func. Mater.*, 2014, **24**, 2572–2590.
- 12 W. Shen, Y. Zhang, P. Wan, L. An, P. Zhang, C. Xiao and X. Chen, *Adv. Mater.*, 2020, **32**, 2001108–2001117.
- 13 Z. Zhang, C. He, Y. Rong, H. Ren, T. Wang, Z. Zou and X. Chen, *Nat. Sci. Rev.*, 2020, 128–139.
- 14 M. M. Avedesian and H. Baker, *ASM specialty handbook: magnesium and magnesium alloys*, ASM International, 1999.
- 15 I. O. F., *ISO-2049: Paints and varnishes — Cross-cut test*, 2013.
- 16 I. O. F., *ISO-8407: Corrosion of metal and alloys — Removal of corrosion products from corrosion test specimens*, 2009.
- 17 B. Peng and A. Imhof, *Soft Matter*, 2015, **11**, 3589–3598.
- 18 B. Dyett and R. Lamb, *Adv. Mater. Interfaces*, 2016, **3**, 1500680–1500689.
- 19 N. Li, Y. Chen, B. Deng, J. Yue, W. Qu, H. Yang, Y. He, W. Xia and L. Li, *J. Alloys Compd.*, 2019, **792**, 1036–1044.
- 20 A. S. Hamdy, *Mater. Lett.*, 2006, **60**, 2633–2637.
- 21 H.-W. Kim, Y.-H. Koh, L.-H. Li, S. Lee and H.-E. Kim, *Biomaterials*, 2004, **25**, 2533–2538.
- 22 D.-M. Liu, Q. Yang and T. Troczynski, *Biomaterials*, 2002, **23**, 691–698.
- 23 H.-W. Kim, Y.-M. Kong, C.-J. Bae, Y.-J. Noh and H.-E. Kim, *Biomaterials*, 2004, **25**, 2919–2926.
- 24 M. L. Zheludkevich, R. Serra, M. F. Montemor, K. A. Yasakau, I. M. M. Salvado and M. G. S. Ferreira, *Electrochim. Acta*, 2005, **51**, 208–217.
- 25 S. H. Messaddeq, S. H. Pulcinelli, C. V. Santilli, A. C. Guastaldi and Y. Messaddeq, *J. Non-Cryst. Solids*, 1999, **247**, 164–170.
- 26 D. Wang and G. P. Bierwagen, *Prog. Org. Coat.*, 2009, **64**, 327–338.
- 27 M. Forsyth, P. C. Howlett, S. K. Tan, D. R. MacFarlane and N. Birbilis, *Electrochem. Solid-State Lett.*, 2006, **9**, B52–B55.
- 28 N. T. Kirkland, T. Schiller, N. Medhekar and N. Birbilis, *Corros. Sci.*, 2012, **56**, 1–4.
- 29 C. Ke, Y. J. Wu, Y. Qiu, J. H. Duan, N. Birbilis and X. B. Chen, *Corros. Sci.*, 2016, **113**, 145–159.
- 30 G. Q. Duan, L. X. Yang, S. J. Liao, C. Y. Zhang, X. P. Lu, Y. E. Yang, B. Zhang, Y. Wei, T. Zhang, B. X. Yu, X. C. Zhang and F. H. Wang, *Corros. Sci.*, 2018, **135**, 197–206.
- 31 Z. Chunyan, L. Shangju, Y. Baoxing, L. Xiaopeng, C. Xiao-Bo, Z. Tao and W. Fuhui, *Corros. Sci.*, 2019, **150**, 279–295.
- 32 X. Lu, Y. Li, P. Ju, Y. Chen, J. Yang, K. Qian, T. Zhang and F. Wang, *Corros. Sci.*, 2019, **148**, 264–271.
- 33 G. Wu, X. Zhang, Y. Zhao, J. M. Ibrahim, G. Yuan and P. K. Chu, *Corros. Sci.*, 2014, **78**, 121–129.
- 34 M. A. Shaik, K. H. Syed and B. R. Golla, *Corros. Sci.*, 2019, **153**, 249–257.
- 35 H. Qian, D. Xu, C. Du, D. Zhang, X. Li, L. Huang, L. Deng, Y. Tu, J. M. Mol and H. A. Terry, *J. Mater. Chem. A*, 2017, **5**, 2355–2364.
- 36 Q. Hou, Z. Liu, C. Li and X. Li, *Corros. Sci.*, 2017, **128**, 154–163.

